www.czasopisma.pan.pl PAN www.journals.pan.pl

ARCHIVES of FOUNDRY ENGINEERING

ISSN (2299-2944)
Volume 21
Issue 1/2021

119 – 124

10.24425/afe.2021.136087

17/1

Published quarterly as the organ of the Foundry Commission of the Polish Academy of Sciences

Oxide Layer Evolution of Cast Fe24Cr12NiXNb Heat-Resistant Cast Steels at 900°C in Atmospheric Air

P.A. Ramos [a,b,] *, R.S. Coelho [c], H.C. Pinto [d], F. Soldera [e], F. Mücklich [e], P.P. Brito [a]

[a] Pontifical Catholic University of Minas Gerais, Brazil
[b] Federal Institute of Science and Technology of Minas Gerais, Brazil
[c] SENAI CIMATEC, Institute of Innovation for Forming and Joining of Materials, Av. Orlando Gomes, 1845, Piatã, 41650-010, Salvador-BA, Brazil
[d] Department of Materials Engineering - SMM, São Carlos School of Engineering – EESC, University of São Paulo – USP, São Carlos, SP, Brazil
[e] Chair of Functional Materials, Department of Materials Science, Saarland University, 66123, Saarbrücken, Saarland, Germany
* Corresponding author. E-mail address: Pedroaugustoramos@hotmail.com

Received 16.12.2020; accepted in revised form 24.02.2021

Abstract

The austenitic stainless steels are a group of alloys normally used under high mechanical and thermal requests, in which high temperature oxidation is normally present due to oxygen presence. This study examines the oxide layer evolution for Fe24Cr12NiXNb modified austenitic stainless steel A297 HH with 0,09%Nb and 0,77%Nb content at 900°C under atmospheric air and isothermal oxidation. The modifiers elements such as Mo, Co and Ti, added to provide high mechanical strength, varied due to the casting procedure, however main elements such as Cr, Ni, Mn and Si were kept at balanced levels to avoid microstructure changing. The oxide layer analysis was performed by confocal laser scanning microscopy (CLS) and scanning electron microscopy (SEM). The elemental analysis of the different phases was measured with energy dispersive X-ray spectroscopy (EDX). The Nb-alloyed steel generated a thicker Cr oxide layer. Generally elemental Nb did not provide any noticeable difference in oxide scale growth, for the specific range of Nb amount and temperature studied. High temperature oxidation up to 120h was characterized by protective Cr oxidation, after this period a non-protective Fe-based oxidation took place. Cr, Fe and Ni oxides were observed in the multilayer oxide scale.

Keywords: Austenitic heat-resistant cast steels, Microstructure, Nb-alloyed Steels, Oxide Scale, High Temperature Oxidation

1. Introduction

Austenitic heat resistant cast stainless steels (ASTM A297) are commonly used in reformer furnaces, petrochemical industry and nuclear power plants (~900°C) due to their high oxidation and mechanical resistance at elevated temperatures [1]. These steels have usually Fe, Cr, and Ni as main alloy elements, with some other elements in small amounts to improve, among others, mechanical properties [1–7].

The high temperature oxidation resistance supposes to be obtained by the formation of a protective barrier (oxide scale) between gaseous atmosphere and metal substrate. The oxidation

resistance can be achieved, if a good maintenance of this scale and its stability is ensured [8]. Li *et al.* [9] showed that the oxidation behavior depends on several mixed factors such as microstructure, chemical composition of the substrate as well as oxidation condition (isothermal or cyclic) [9–12].
The most extensively investigated class of cast A297 steel , is HP grade, since it has good mechanical behavior (the higher Ni content the better the creep properties in comparison with other A297 grades) [13–15]. The A297 HH steel is an alternative with lower nickel content compared to HP and HK grades, having general composition Fe24Cr12NiχNb (in wt%), and having been developed for better cost-benefit without neglecting its performance. The reduction in Ni content, which consequently produces a decrease in creep properties, requires the increment of new elements such as Co, Ti, and Nb to enhance mechanical properties. In last years the Nb addition has been investigated with the objective of increasing high temperature strength by the precipitation of Nb carbides[1] in the austenitic matrix.

The addition of niobium may change carbide fraction (normally Cr_7C3 and $Cr_{23}C_6$) modifying the Cr content in solution. However, the oxide scale evolution depending on the Nb additions is not fully understood [2]. The understanding of oxidation mechanisms and oxide layer development is an important issue closely related with microstructure[16], oxidation properties [17] and improvement in the material life cycle. Since we have a new modified steel , in the present work an experimental investigation was carried out in order to characterize the oxide scale evolution of this Fe24Cr12NiχNb steel (A297 modified HH steel) at 900°C under atmospheric air on isothermal oxidation which is considered the standard conditions in most field applications.

2. Experimental procedure

The austenitic stainless steel A297 Gr. HH modified (Fe24Cr12Ni) with different Nb contents used in the present study were produced by FULIG® casting company and are currently used in high temperature applications. The heat-resistant cast austenitic stainless steels were characterized by chemical composition, as presented in Table 1, by using spectrometer SHIMADZU OES 5500 II. They will be called samples 0,09%Nb and 0,77%Nb.

The percentages of alloying elements were all of them within A297 standard limits, as well as the levels of impurities, such as P and S.

The long-term high temperature oxidation experiments were performed in a muffle furnace for different isothermal conditions at 900 °C under room air with the different checking times of 1h, 5h, 10h, 24h, 48h, 120h, 240h, 480h and 960h and the samples were previously polished (Up to SiC grade 600). Foremost, the generated raw oxide layers were characterized by Olympus OLS4100 confocal 3D laser scanning microscopy (CLM).

Table 1.
Chemical composition of the materials employed in the study (values in weight %)

A297 - HH	0.77% Nb	0.09% Nb	Stand. limits A297(max.)
C (mod.*)	0.73	0.89	0.2-0.5
Si	0.97	1.22	2.00
Mn	0.55	0.50	2.00
P	0.01	0.03	0.04
S	0.02	0.03	0.04
Ni	11.09	12.12	11.0-14.0
Cr	24.79	24.42	24.0-28.0
Mo	0.32	0.12	0.5
Co (mod.*)	0.28	0.47	-
Nb (mod.*)	0.77	0.09	-
Ti (mod.*)	0.10	0.01	-
Fe	60.32	59.74	Balance

**Mod.: modified*

Then, the cross sections were prepared and covered with plasma sputtering process with 8% Au + 20% Pd at argon pressure of 0,02 mbar, 20-25 mA current for 5 minutes resulting in a 20nm layer making the oxide scale electrically conductive. Thus, electrochemical copper deposition could be done with a copper sheet immersed in a copper solution (20g $CuSO_4$ + 100gH_2O) at 1,5V(DC) for 15 min which generated a copper layer above the oxide around 10µm, that is mandatory to avoid oxide scale spallation due to preparation before mounting in conductive resin. Then, metallographic sample preparation was performed up to 0,05 µm with alumina solution at vibratory polisher machine (VIBROMET 2 - BUEHLER) without etching. The three pieces of each sample were measured in order to provide statistics. Samples for microstructural analysis and oxidation tests were cut from the cast blocks with cubic dimensions of 10 x 10 x 10 mm.

The oxide scale morphology, cross section and chemical elements distribution was characterized by a dual-beam focused ion beam/scanning electron microscopy (FIB/SEM) workstation (FEI Helios NanoLab 600) equipped with EDAX energy dispersive X-ray spectroscopy module (EDX).

3. Results and discussion

3.1. Alloys microstructure

Optical micrographs obtained from the microstructure of the samples 0.09%Nb and 0.77%Nb are presented in Figure 1. They exhibit differences regarding precipitation and dendritic form. The austenitic matrix contains Cr and also Nb/Ti precipitates mainly seen in 0.77%Nb alloy.

In Figure 1(a) the microstructure of the 0.09%Nb alloy is presented revealing precipitates with the typical morphology of primary Cr carbides. In Figure 1(b) the microstructure of the 0.77%Nb alloy is shown, exhibiting the same primary Cr carbides

along with new precipitates which were precipitated by the increase in niobium and titanium content.

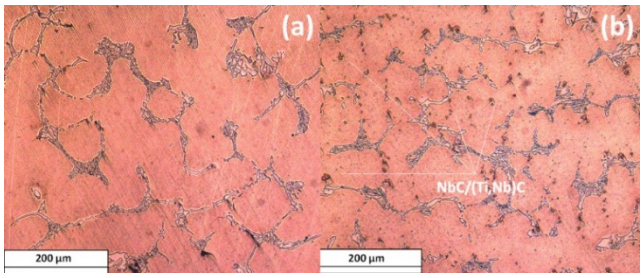

Fig. 1. Optical micrograph of 0.09%Nb(a) and 0.77%Nb(b) alloy

Nb addition provide bigger carbide precipitation and, in this research, we investigated the oxide layer formation during high temperature oxidation in order to analyze whether microstructural changes affects oxide layer formation or not.

3.2. Oxide layer evolution and morphology

Considering optical laser micrographs obtained from samples 0.09%Nb and 0.77%Nb which are presented in Figure 2 (superficial morphology) and were obtained from samples after cooling and before plasma sputtering covering (as oxidized condition), it is possible to see clearly the oxides development starting with thin gold color oxide layer (1h), followed by other layer characterized here by darker tones (5h up to 120h) and finally covered by gray layer (clearly seen after 240h).

The differences between alloys were more significant in 1h and 5h during the beginning of oxidation suggested by chemical composition differences. The oxides have a spinel-like structure, without visible nodules or cracks on the surface. The oxides formation occurs in the form of islands that keep closer and closer until they form a consistent layer. This formation occurs initially in the dendritic boundaries that is a diffusivity favored region initially for Cr ions and later for the Ni and Fe ions as expected in this kind of steels.

The next step was the observation of oxide layer cross sections after metallographic preparation with copper covering and carefully polishing as described in section 2 of this manuscript. Considering optical laser micrographs obtained from samples 0.09%Nb and 0.77%Nb which are presented in Figure 3 (cross-section). Copper covering was more suitable than Ni covering for protecting the scales during polishing.

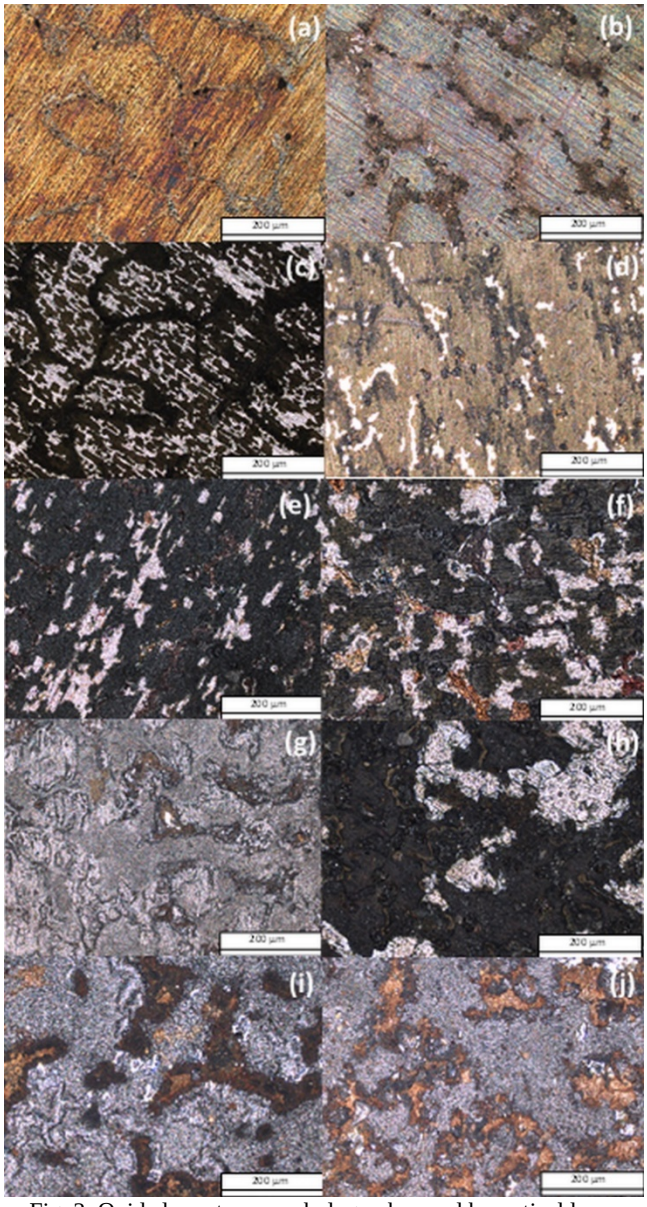

Fig. 2. Oxide layer top morphology observed by optical laser microscopy of samples with 1h(a-b), 5h(c-d), 120h(e-f), 240h(g-h), 960h(i-j) for 0.09%Nb and 0.77%Nb alloy, respectively

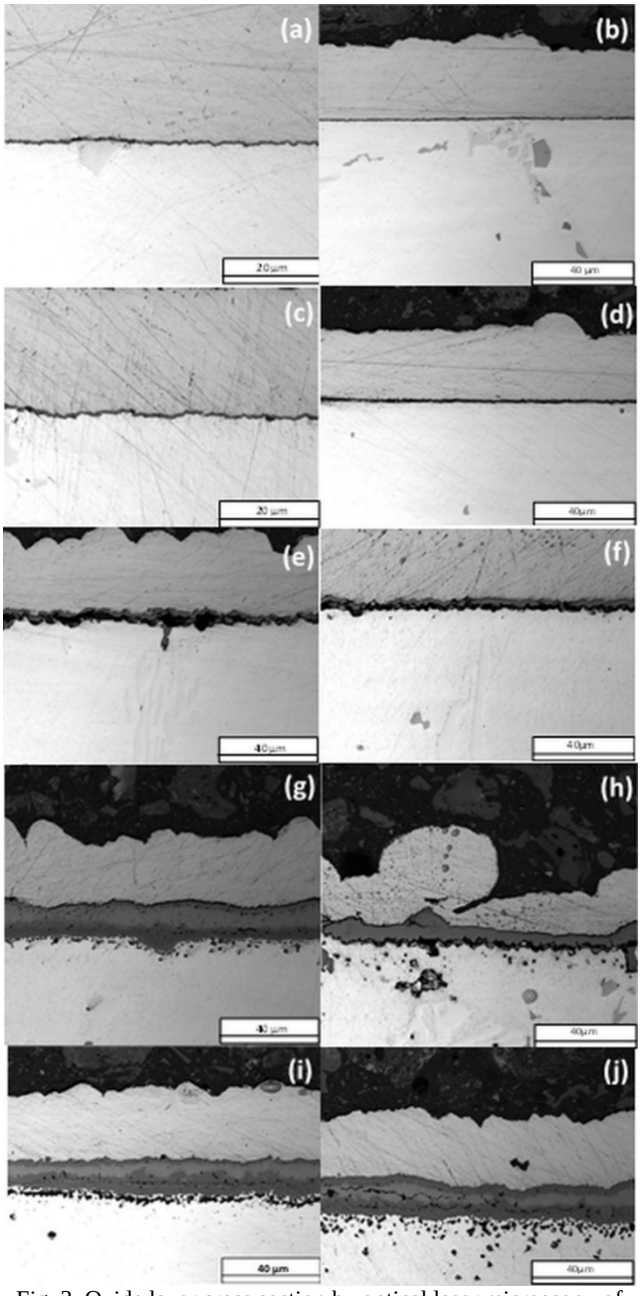

Fig. 3. Oxide layer cross section by optical laser microscopy of samples with 1h(a-b), 5h(c-d), 120h(e-f), 240h(g-h), 960h(i-j) for 0.09%Nb and 0.77%Nb alloy, respectively

In Figure 3, it is possible to determine an oxide growth evolution starting with 1h up to 960h. The optical contrast suggested also a multilayer oxide scale as predicted by top morphology images and also some cracks are now seen due to residual stress caused by fast cooling rates and differences between oxide and metallic substrate thermal expansion coefficients or even due to polishing procedure.

However, from the cross section it is possible to determine in a better way the growth mechanisms and the position of each type of oxide generated in the scale from the substrate [8].

3.3. Oxide layer microstructure

The superficial morphology and cross section images were co-related with scanning electron micrographs obtained from samples 0.09%Nb and 0.77%Nb which are presented in Figure 4 (secondary electrons mode).

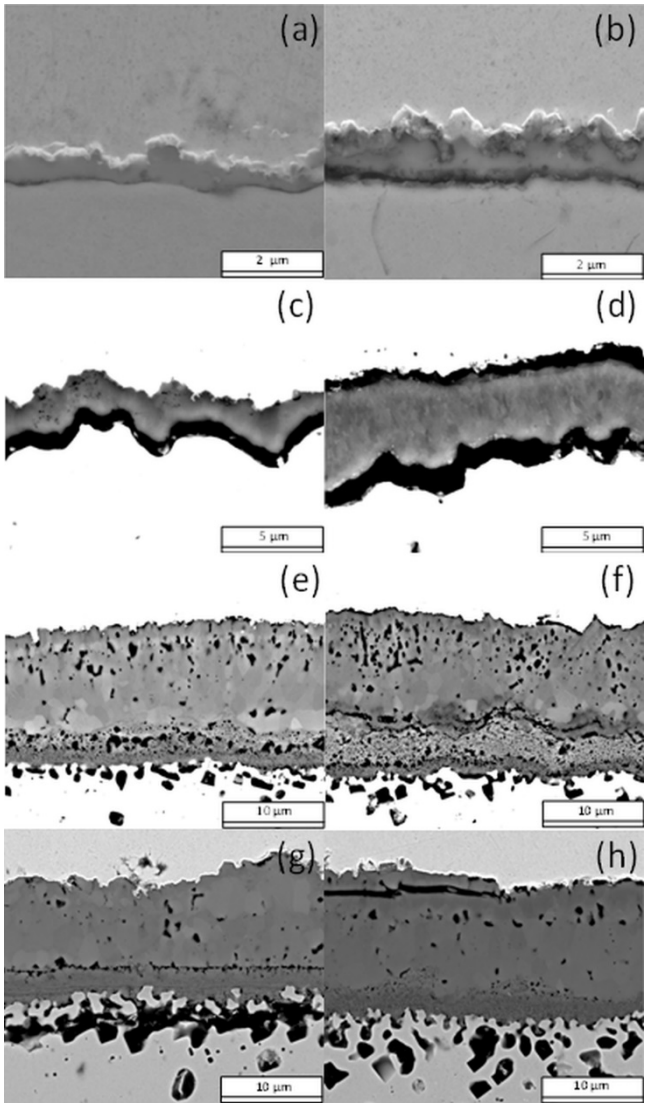

Fig. 4. Oxide layer cross section by scanning electron microscopy of samples 5h(a-b), 120h(c-d), 240h(e-f), 960h(g-h) for 0.09%Nb and 0.77% alloy, respectively

Previous research described through XRD analysis that Cr oxide, magnetite (Cr0.03Fe2.96Ni0.01O4) and hematite were the phases found in both oxide scales here analyzed [17].

For layers up to 120h of oxidation a dense Cr oxide layer is observed which becomes porous overtime, consequently facilitating the others ions diffusion through it. At 240h a multilayer oxide scale is already observed with the appearance of Fe oxides immediately above the Cr oxide. This effect lasts until 960h of oxidation.

Nevertheless, for a more precise knowledge about phase formation and detailed spatial configuration of the phases other techniques related with chemical composition needed be employed like EDX linescans profiles. These analyses can be seen on Figures 5 and 6.

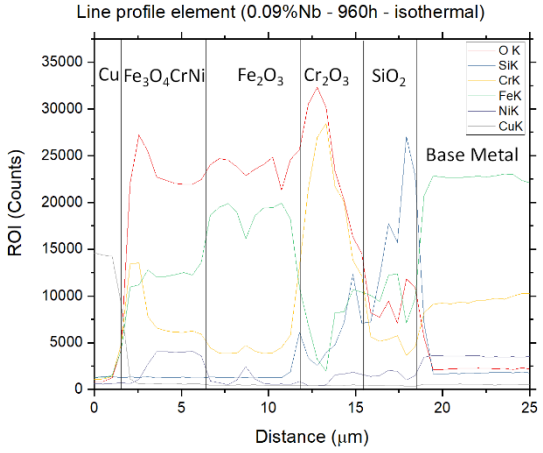

Fig. 5. Oxide layer cross section EDX linescans profile by scanning electron microscopy of samples with 960h of isothermal oxidation, for 0.09%Nb alloy

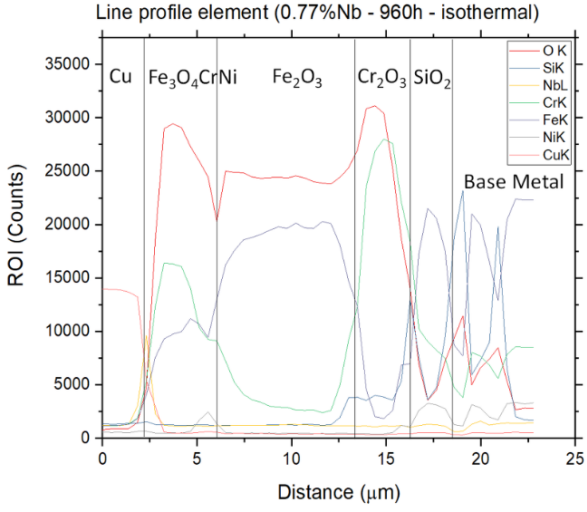

Fig. 6. Oxide layer cross section EDX linescans profile by scanning electron microscopy of samples with 960h of isothermal oxidation, for 0.77%Nb alloy

With these observations was figured out that up to 120h there is a protective oxidation due to slower thickness evolution and to be just one single chemical composition on the scale, in this case, Cr oxide.

After 240h a non-protective oxidation was observed with multilayer generation and faster thickness growth. Detailed information about the oxide layer formation can just be established with EDX linescans profiles of longest time, so approaching all phases generated during the scale formation.

The austenitic heat resistant steels exposed to high temperatures at atmospheric air generates multiple oxide scale with different phases [2]. Ellingham diagrams are reasonable way to get some information about the growth of these scales, but also other factors can influence in which oxides appear first, like ions diffusion, for example.

Basically, the oxides stability at Ellingham diagrams is based on Gibbs free energy in such reaction for oxide formation. The most thermodynamically stable phases are found close to the substrate and are formed first, being necessary also understand the diffusion, as reported by Wagner theory, in high temperature conditions [8,18] to understand the oxides growth sequence.

In the present work, according to Ellingham diagrams the oxide scale predicted formation were Si oxide (SiO_2), Cr oxide (Cr_2O_3), Fe oxide (magnetite and hematite) considering down-top order from the substrate. This correlates reasonably the empirical experiments, as can be seen in Figure 5 and 6. It is worth noticing that the oxide scales formed on pure iron (or carbon steels) is structured (from the substrate upwards) by layers of FeO, Fe_3O_4 and Fe_2O_3. In the present case, the order is inverted because Fe_2O_3 is found closer to the substrate (with Cr_2O_3) due to crystal structure compatibility (Fe_2O_3 and Cr_2O_3 both exhibit rhombohedral crystal structures).

The Si and Cr oxides can be considered as protective scales. The diffusivity through Cr oxide is a determinant factor for the formation of non-protective Fe-based oxides [7], as well as oxygen diffusion through the layer and spallation due to cracks formation when oxide scale is submitted to high stress state due to thermal expansion difference during the cooling cycle [8,17].

4. Conclusions

In the present work, the ASTM A297 Gr. HH modified austenitic heat-resistant cast steels oxide scale evolution containing 0.09%Nb and 0.77%Nb was investigated. The oxide layers' investigation included superficial observation up to use of techniques such as SEM and EDX analysis to identify the phases. The set of all these analyzes allowed the characterization of the layers. The following conclusions could be done:

- The addition of niobium did not impair the oxidation resistance of the modified steel, since no noticeable differences on oxide scales was observed related to microstructural characteristics or different alloys compositions;
- High temperature oxidation up to 120h was characterized by protective Cr oxidation, after this period a non-protective Fe-based oxidation started generating a multilayer oxide scale;

- Si, Cr, Fe and Ni are the main elements present in the oxide scale for both alloys and the growth order could be related with Ellingham diagrams theory.

Acknowledgements

This work was financially supported by the Coordination for the Improvement of Higher Education Personnel – CAPES (grant number 88887.302880/2018-00, PROBRAL project 88881.143948/2017-01 and Finance Code 01) and by the German Academic Exchange Service – DAAD (project DAAD PPP-Brazil 2018 – ID 57390937). The authors are grateful to Mr. Christoph Pauly for assistance with oxide scale copper covering process, K. Aristizabal and M. A. Guitar for SEM/EDX analyses (UdS - Germany).

References

[1] Abbasi, M., Park, I., Ro, Y., Ji, Y., Ayer, R. & Shim, J.H. (2019). G-phase formation in twenty-years aged heat-resistant cast austenitic steel reformer tube. *Materials Characterization.* 148, 297-306. DOI: 10.1016/j.matchar.2019.01.003.

[2] Madern, N., Monnier, J., Baddour-Hadjean, R., Steckmeyer, A. & Joubert, J.M. (2018). Characterization of refractory steel oxidation at high temperature. *Corrosion Science.* 132, 223-233. DOI: 10.1016/j.corsci.2017.12.029.

[3] Kondrat'ev, S.Y., Kraposhin, V.S., Anastasiadi, G.P. & Talis, A.L. (2015). Experimental observation and crystallographic description of M7C3 carbide transformation in Fe-Cr-Ni-C HP type alloy. *Acta Materialia.* 100, 275-281. DOI: 10.1016/j.actamat.2015.08.056.

[4] Dewar, M.P. & Gerlich, A.P. (2013). Correlation between experimental and calculated phase fractions in aged 20Cr32Ni1Nb austenitic stainless steels containing nitrogen. *Metallurgical and Materials Transactions A.* 44, 627-639. DOI: 10.1007/s11661-012-1457-1.

[5] Pascal, C., Braccini, M., Parry, V., Fedorova, E., Mantel, M., Oquab, D. & Monceau, D. (2017). Relation between microstructure induced by oxidation and room-temperature mechanical properties of the thermally grown oxide scales on austenitic stainless steels. *Materials Characterization.* 127, 161-170. DOI: 10.1016/j.matchar.2017.03.003.

[6] Chen, H., Wang, H., Sun, Q., Long, C., Wei, T., Kim, S.H., Chen, J., Kim, C., & Jang, C. (2018). Oxidation behavior of Fe-20Cr-25Ni-Nb austenitic stainless steel in high-temperature environment with small amount of water vapor. *Corrosion Science.* 145, 90-99. DOI: 10.1016/j.corsci.2018.09.016.

[7] Zhang, X., Li, D., Li, Y. & Lu, S. (2019). Effect of aging treatment on the microstructures and mechanical properties evolution of 25Cr-20Ni austenitic stainless steel weldments with different Nb contents. *Journal of Materials Science & Technology.* 35, 520-529. DOI: 10.1016/j.jmst.2018.10.017.

[8] Birks, N., Meier, G.H. & Pettit, F.S. (2006). Introduction to the high temperature oxidation of metals, Second edition. *Cambridge university press.* DOI: 10.1017/CBO9781139163903.

[9] Li, D.S., Dai, Q.X., Cheng, X.N., Wang, R.R. & Huang, Y. (2012). High-temperature oxidation resistance of austenitic stainless steel Cr18Ni11Cu3Al3MnNb. *Journal of Iron Steel Research International.* 19, 74-78. DOI: 10.1016/S1006-706X(12)60103-4.

[10] Kaya, A.A. (2002). Microstructure of HK40 alloy after high-temperature service in oxidizing/carburizing environment: II. Carburization and carbide transformations. *Materials Characterization.* 49, 23-34. DOI: 10.1016/S1044-5803(02)00284-X.

[11] Li, H., Zhang, B., Jiang, Z., Zhang, S., Feng, H., Han, P., Dong, N., Zhang, W., Li, G., Fan, G. & Lin, Q. (2016). A new insight into high-temperature oxidation mechanism of super-austenitic stainless steel S32654 in air. *Journal of Alloys and Compounds.* 686, 326-338. DOI: 10.1016/j.jallcom.2016.06.023.

[12] M. Salehi Doolabi, B. Ghasemi, S.K. Sadrnezhaad, A. Feizabadi, A. HabibollahZadeh, D. Salehi Doolabi, M. AsadiZarch. (2017). Comparison of Isothermal with cyclic oxidation behavior of "Cr-Aluminide" coating on inconel 738LC at 900 °C. *Oxidation of Metals.* 87, 57-74. DOI: 10.1007/s11085-016-9657-5.

[13] De Almeida, L.H., Ribeiro, A.F. & Le May, I. (2002). Microstructural characterization of modified 25Cr-35Ni centrifugally cast steel furnace tubes. *Materials Characterization.* 49, 219-229. DOI: 10.1016/S1044-5803(03)00013-5.

[14] Nishimoto, K., Saida, K., Inui, M. & Takahashi, M. (2001). Changes in microstructure of HP-modified, heat-resisting cast alloys under long-term aging. Repair weld cracking of service-exposed, HP-modified, heat-resisting cast alloys (2nd report). *Welding International.* 15(7), 509-517. DOI: 10.1080/ 09507110109549397.

[15] Joubert, J.M., St-Fleur, W., Sarthou, J., Steckmeyer, A. & Fournier, B. (2014). Equilibrium characterization and thermodynamic calculations on highly alloyed refractory steels. *Calphad Comput. Coupling Phase Diagrams Thermochem.* 46, 55-61. DOI: 10.1016/j.calphad.2014.02.002.

[16] Ramos, P.A., Coelho, R.S., Pinto, H.C., Soldera, F., Mücklich, F. & Brito, P. (2021). Microstructure and cyclic oxidation behavior of modified Nb-alloyed A297 HH refractory austenitic stainless steel. *Materials Chemistry and Physics.* 263, 124361. DOI: 10.1016/j.matchemphys.2021.124361.

[17] Ramos, P.A., Coelho, R.S., Soldera, F., Pinto, H.C., Mücklich, F. & Brito,P. (2020). Residual stress analysis in thermally grown oxide scales developed on Nb-alloyed refractory austenitic stainless steels. *Corrosion Science.* 178, 109066. DOI: 10.1016/j.corsci.2020.109066.

[18] McCafferty E. (2010). Introduction to corrosion science. *Springer Science & Business Media.* DOI: 10.1007/978-1-4419-0455-3.